Moisture Asymmetry and MJO Eastward Propagation in an Aquaplanet General Circulation Model*

PANG-CHI HSU AND TIM LI

CDRC/ESMC, International Laboratory on Climate and Environment Change, Nanjing University of Information Science and Technology, Nanjing, China, and International Pacific Research Center, School of Ocean and Earth Science and Technology, University of Hawai'i at Mānoa, Honolulu, Hawaii

HIROYUKI MURAKAMI

International Pacific Research Center, School of Ocean and Earth Science and Technology, University of Hawai'i at Mānoa, Honolulu, Hawaii, and Climate Research Department, Meteorological Research Institute, Tsukuba, Japan

(Manuscript received 21 February 2014, in final form 12 July 2014)

ABSTRACT

The role of zonal moisture asymmetry in the eastward propagation of the Madden–Julian oscillation (MJO) is investigated through a set of aquaplanet atmospheric general circulation model (AGCM) experiments with a zonally symmetric sea surface temperature distribution. In the control experiment, the model produces eastward-propagating MJO-like perturbations with a dominant period of 30–90 days. The model MJO exhibits a clear zonal asymmetry in the lower-tropospheric specific humidity field, with a positive (negative) anomaly appearing to the east (west) of the MJO convection. A diagnosis of the lower-tropospheric moisture budget indicates that the asymmetry primarily arises from vertical moisture advection associated with boundary layer convergence, while horizontal moisture advection has the opposite effect.

In a sensitivity experiment, the lower-tropospheric specific humidity field is relaxed toward a zonal-mean basic state derived from the control simulation. In this case, the model's mean state remains the same, but its intraseasonal mode becomes quasi-stationary. The numerical model experiments clearly demonstrate the importance of the zonal moisture asymmetry in MJO eastward propagation.

1. Introduction

The Madden–Julian oscillation (MJO; Madden and Julian 1971, 1972) is a leading mode of intraseasonal variability in the tropics, characterized by the eastward propagation of planetary-scale coupled circulation–convection patterns [Wang and Rui (1990); Li and Zhou (2009); see Li (2014) for the latest review of this subject]. The structure of the MJO can be regarded as a first-baroclinic Kelvin–Rossby wave couplet in the free atmosphere and a zonal phase leading of convergence (Hendon and Salby 1994; Li and Wang 1994; Wang and Li 1994; Maloney and Hartmann 1998) and moisture (Sperber 2003; Kiladis et al. 2005; Benedict and Randall 2007) in the planetary boundary layer (PBL).

Recent studies emphasized the role of moisture dynamics in the eastward propagation of the MJO (e.g., Maloney 2009; Hsu and Li 2012; Sobel and Maloney 2013). By analyzing column-integrated moist static energy (MSE) and moisture budgets from a general circulation model, Maloney (2009) indicated that the horizontal advection dominates the positive MSE/moisture anomaly to the east of the MJO convection. Based on a PBL-integrated moisture diagnosis using observations, Hsu and Li (2012) showed that the

* Earth System Modelling Center Contribution Number 016, School of Ocean and Earth Science and Technology Contribution Number 9195, and International Pacific Research Center Contribution Number 1075.

Corresponding author address: Tim Li, IPRC, SOEST, University of Hawai'i at Mānoa, 1680 East West Road, Post Bldg. 401, Honolulu, HI 96822.
E-mail: timli@hawaii.edu

DOI: 10.1175/JCLI-D-14-00148.1

© 2014 American Meteorological Society

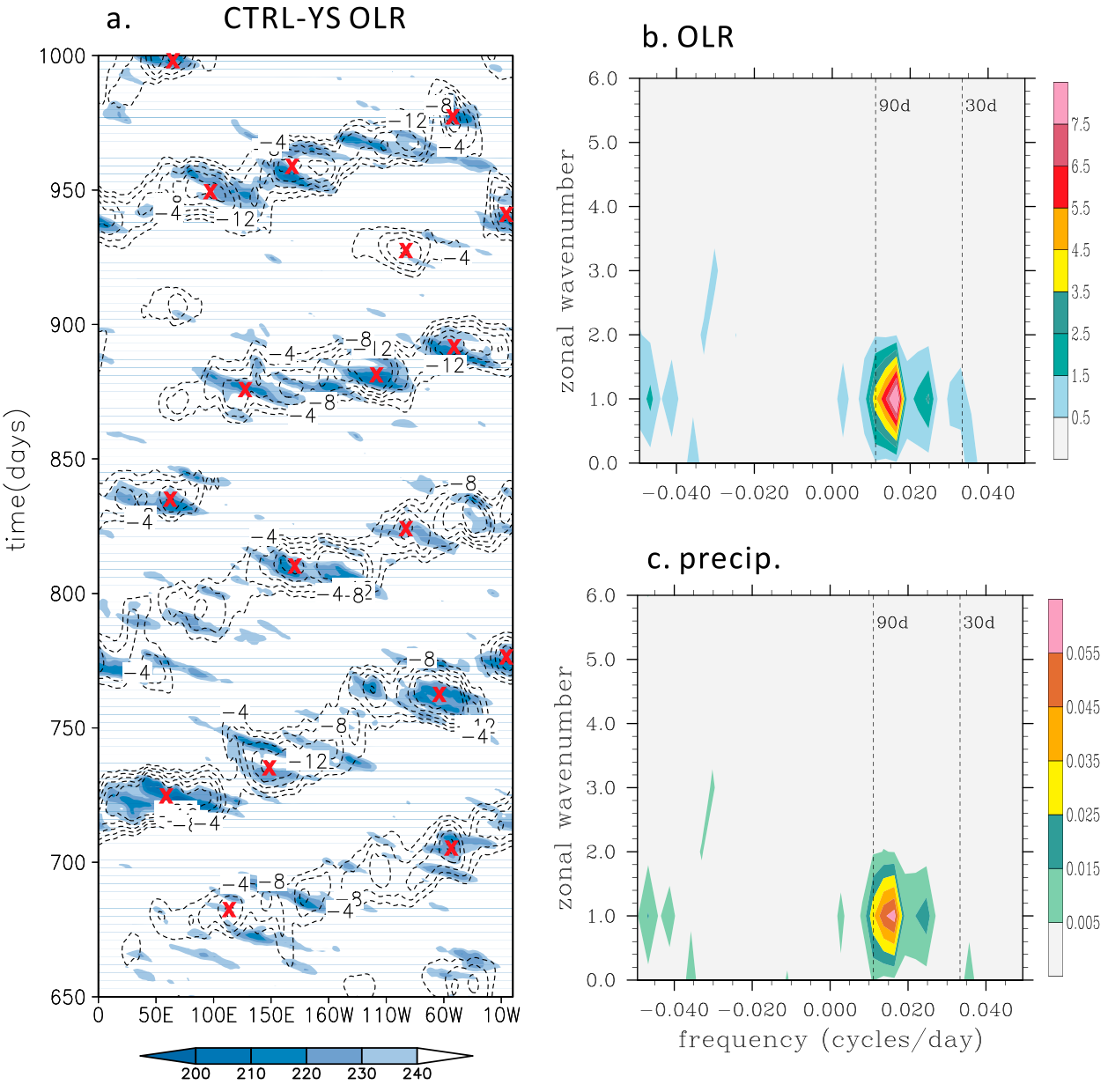

FIG. 1. (a) Time–longitude section of 10°S–10°N averaged unfiltered OLR (shading; W m^{-2}) and 30–90-day filtered OLR (contour; W m^{-2}) for a 350-day segment during 10-yr integration period in the CTRL. Wavenumber–frequency spectra of 10°S–10°N averaged (b) OLR and (c) precipitation from the 10-yr integration of the CTRL. Red crosses in (a) mark the locations of MJO convective centers selected for the composite analysis.

vertical advection associated with PBL convergence is essential to cause the moisture asymmetry, which is characterized by Sperber (2003) and Kiladis et al. (2005). It has been shown that the lower-tropospheric moistening ahead of the convection could destabilize the atmosphere by increasing the MSE and the setup of a convectively unstable stratification, preconditioning the eastward propagation of the MJO (Kemball-Cook and Weare 2001; Benedict and Randall 2007; Hsu and Li 2012).

A key question related to MJO dynamics is whether or not the convectively coupled Kelvin–Rossby wave couplet can propagate eastward in the absence of zonal asymmetry of moisture. A simple 2.5-layer atmospheric model of Wang and Li (1994) can support an eastward-propagating mode even under a zonally

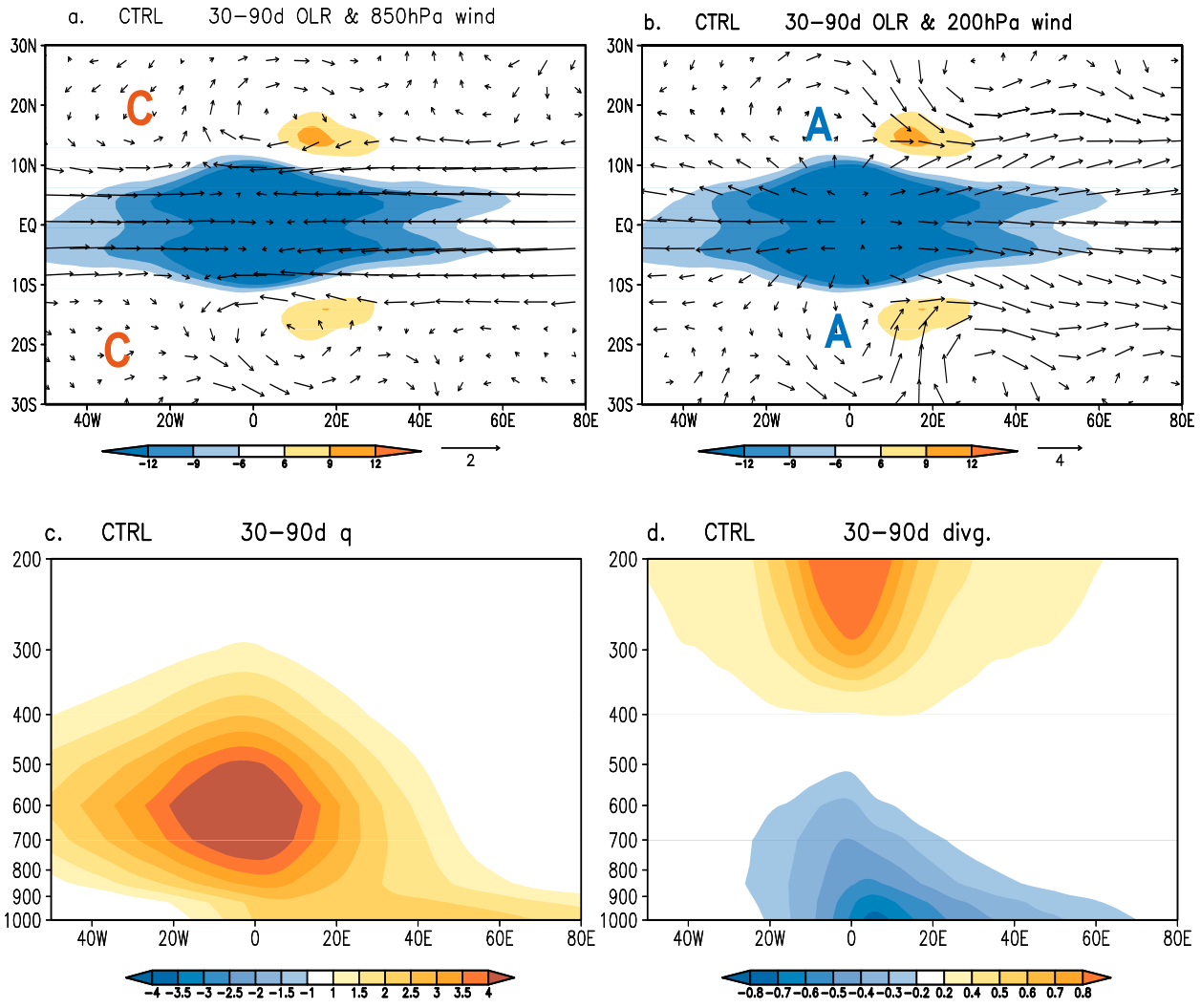

FIG. 2. (top) Composite patterns of 30–90-day filtered OLR (shading; $W\,m^{-2}$) and wind fields (vectors; $m\,s^{-1}$) at (a) 850 hPa and (b) 200 hPa in the CTRL. (bottom) Zonal–vertical distributions of 10°S–10°N averaged 30–90-day filtered (c) specific humidity ($10^{-4}\,kg\,kg^{-1}$) and (d) divergence ($10^{-6}\,s^{-1}$) in the CTRL. The composite OLR center is located at 0° on the horizontal axis. Letters "C" and "A" in (a),(b) represent cyclonic and anticyclonic anomalies, respectively.

symmetric moisture condition. To verify the role of the perturbation moisture asymmetry in MJO eastward propagation, we conduct control and sensitivity experiments using an aquaplanet atmospheric general circulation model (AGCM) that retains full physics but discards the complexity induced by lower boundary conditions, including land–sea distribution, topography, and spatially varying sea surface temperature (SST) distribution. Aquaplanet AGCMs forced by idealized SST patterns simplify model behaviors and have been widely used to investigate fundamental dynamics associated with the MJO (e.g., Hayashi and Sumi 1986; Lee et al. 2003; Maloney et al. 2010; Andersen and Kuang 2012). Model description and experimental designs are described in section 2. Control simulation of the MJO feature and diagnosis of moisture budget are presented in section 3. Section 4 shows the result of a sensitivity simulation in which the moisture asymmetry of lower troposphere is suppressed. In section 5, additional simulations are performed to demonstrate that our conclusions are independent of convection schemes used. A summary and discussion are given in section 6.

2. Model and experimental design

The model used in this study is adapted from the Japan Meteorological Research Institute (MRI)-AGCM, version

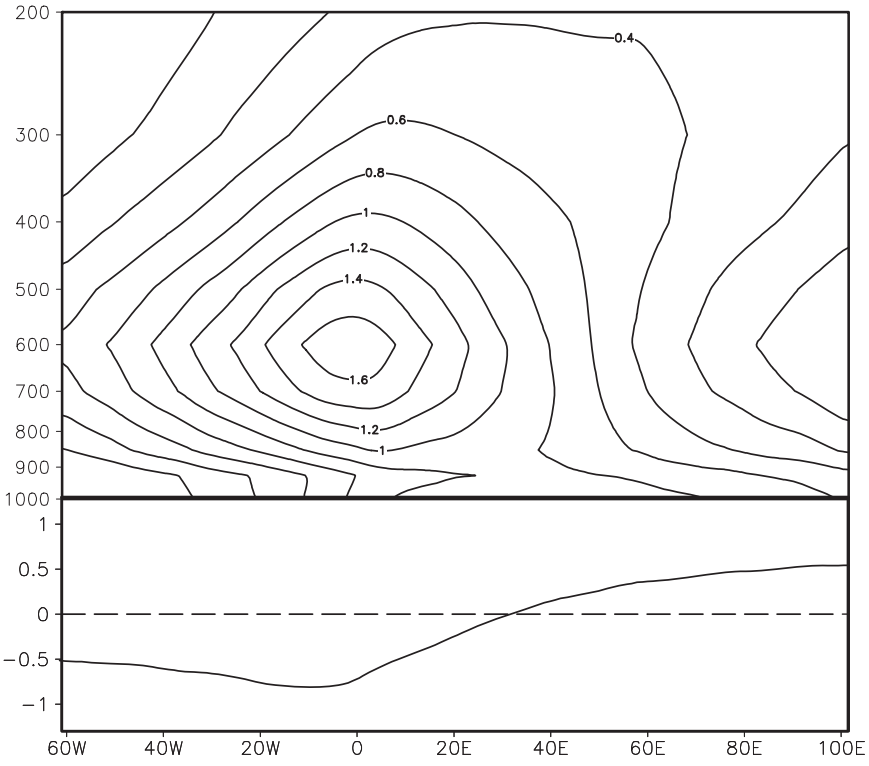

FIG. 3. Zonal–vertical distribution of 10°S–10°N averaged (top) 30–90-day filtered equivalent potential temperature and (bottom) convective instability index, which is defined as the difference of 30–90-day filtered equivalent potential temperature in the PBL (1000–800 hPa) and middle troposphere (600–400 hPa) in the CTRL. Units are in kelvin.

3.2 (MRI-AGCM3.2), at a linear spectral T_L159 resolution (~120 km). This is the newest version of the MRI-AGCM with an upgraded cumulus parameterization, named the Yoshimura cumulus scheme (Yoshimura et al. 2014). The Yoshimura scheme allows the existence of multiple convective updrafts with different heights (similar to Arakawa and Schubert 1974) but considers a more detailed entraining and detraining plume (in a way similar to Tiedtke 1989). Using the new cumulus parameterization, the MRI-AGCM3.2 substantially improves the simulations of tropical precipitation and circulations from the older version of MRI-AGCM3.1, which used the Arakawa–Schubert cumulus scheme. Details of MRI-AGCM3.2 physics and performance were documented in Mizuta et al. (2012).

The SST field for the aquaplanet simulation is derived from the zonal average of the hemisphere-symmetric climatological SST in September when the SST has the maximum at the equator, from the Hadley Centre Sea Ice and Sea Surface Temperature dataset (HadISST1; Rayner et al. 2003). (This idealized SST distribution is shown in Fig. 7a.) The solar radiation at the top of the atmosphere is fixed at the equinox. This experiment is referred to as the control (CTRL).

To test the hypothesis that the zonal moisture asymmetry is critical for MJO propagation, a sensitivity experiment is designed, in which we use the same setting as in the CTRL but damp the model specific humidity field at low levels toward a zonal-mean specific humidity field derived from the CTRL. The time scale of the Newtonian damping is set at 0.5 days between 1000 and 800 hPa. The Newtonian damping coefficient is set to zero above 700 hPa, and is linear between 800 and 700 hPa. By doing so, the perturbation moisture tends to be zero (without the feature of zonal asymmetry about the MJO convective center) in the lower troposphere while allowing the PBL convergence to be asymmetric. This experiment is referred to as q-damping (QD). Both the CTRL and QD are integrated for 10 yr after model has reached its quasi–steady state (after a 6-month spinup).

3. MJO in the control simulation

Figure 1 shows the characteristics of simulated outgoing longwave radiation (OLR) and precipitation in the CTRL. The OLR field consistently reveals the

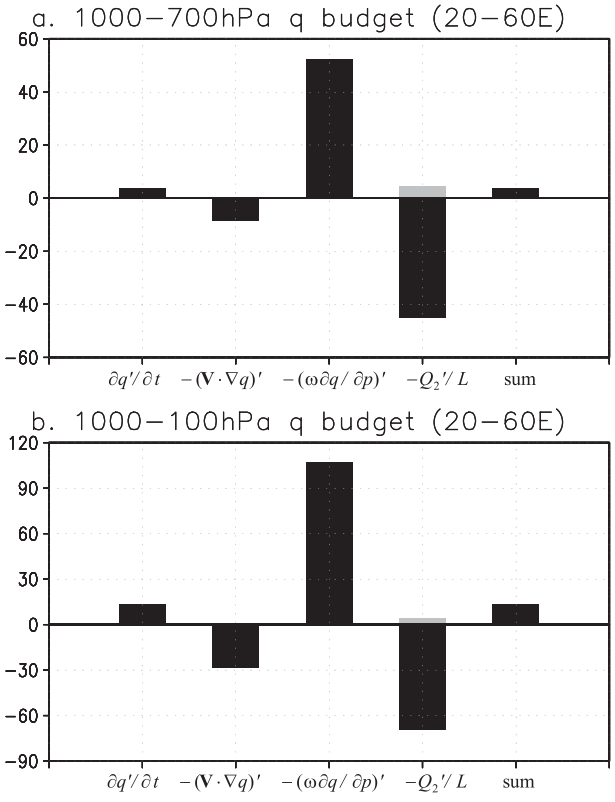

FIG. 4. (a) Lower-tropospheric (1000–700 hPa) integrated and (b) column (1000–100 hPa) integrated intraseasonal (30–90 day) moisture budget terms (10^{-7} kg m^{-2} s^{-1}) over the anomalous moistening region (20°–60° to the east of the MJO convective center) in the CTRL. From left to right, the model specific humidity tendency, horizontal moisture advection, vertical moisture advection, latent heating including surface evaporation (gray bar), and the sum of the last three terms.

eastward-propagating features along the equator (Fig. 1a). The maximum spectra of both OLR and precipitation appear near zonal wavenumber 1 and at the period of 30–90 days (Figs. 1b and 1c), resembling the observed MJO. The simulation also generates the multiscale nature of the observed MJO (Nakazawa 1988). Within the low-frequency eastward-propagating MJO convective envelops, embedded westward-propagating synoptic convective events are active (Fig. 1a).

A composite analysis is conducted to reveal the MJO structures in the CTRL. A 30–90-day bandpass filter is applied to extract the MJO signals. The strong MJO events are defined by the 30–90-day filtered OLR averaged over 10°S–10°N exceeding −1 standard deviation (marked by red crosses in Fig. 1a). Based on this criterion, 134 cases are selected during the 10-yr integration. Then, all the cases are composited based on the OLR centers. The composited circulation in the CTRL displays a baroclinic Kelvin–Rossby wave couplet structure in response to the MJO heating (Figs. 2a and 2b). This structure agrees well with the observation (e.g., Salby et al. 1994). To the east of the MJO convection, easterly (westerly) flows associated with the Kelvin wave response appear in the lower (upper) troposphere. To the west of the MJO convection, two cyclonic (anticyclonic) Rossby wave gyres occur in the lower (upper) troposphere on both sides of the equator, accompanied by westerly (easterly) flows near the equator. However, the Rossby gyres in the model are weaker than those observed (Salby et al. 1994). Figures 2c and 2d show the vertical–zonal distributions of MJO moisture and divergence fields. The model simulates well the vertically tilted moisture and divergence structures, similar to the observations (e.g., Kiladis et al. 2005; Hsu and Li 2012). A marked zonal asymmetry appears in the lower-tropospheric moisture and convergence fields, with a positive moisture anomaly and a convergence anomaly appearing to the east of the convection center (Figs. 2c and 2d).

In the observation, the moisture asymmetry plays a crucial role in the eastward propagating of the MJO through inducing the atmospheric destabilization to the east of MJO convection (Hsu and Li 2012). To confirm the effects of moisture asymmetry on the MJO propagation in the model, we examine the vertical profile of the 30–90-day equivalent potential temperature (θ_e'). Consistent with the low-level moistening, θ_e' is found to be increased in the lower troposphere ahead on the MJO convection (Fig. 3). This leads to an increased (decreased) convective instability parameter, defined as the difference of θ_e' between the lower and middle troposphere, and sets up a relatively unstable (stable) stratification to the east (west) of the MJO convection. Thus, the model MJO propagates eastward.

To reveal the processes responsible for the zonal moisture asymmetry in the model, we conduct a vertically integrated moisture budget analysis in the region east of the MJO convection using the following moisture tendency equation:

$$\frac{\partial q'}{\partial t} = -(\mathbf{V}\cdot\nabla q)' - \left(\omega\frac{\partial q}{\partial p}\right)' - \frac{Q_2'}{L}, \qquad (1)$$

where the prime represents vertically integrated quantities associated with the MJO, q is the specific humidity, t is the time, $\mathbf{V}$ is the horizontal wind vector, ∇ is the horizontal gradient operator, p is the pressure, ω is the vertical pressure velocity, L is the latent heat of condensation, and Q_2 is the atmospheric apparent moisture sink (Yanai et al. 1973) that includes net latent heating and vertical convergence of eddy moisture transport.

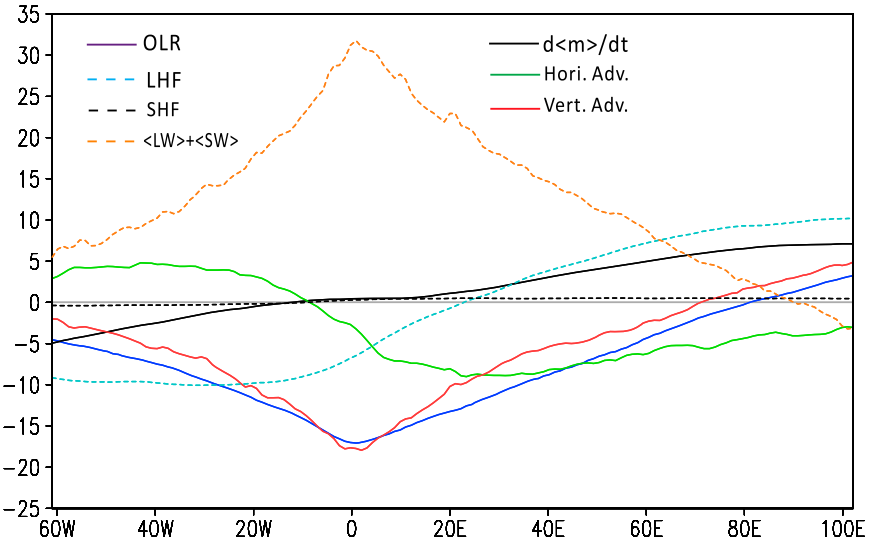

FIG. 5. Composite of vertically integrated 30–90-day MSE budget terms (W m^{-2}) in relation to the MJO convection in the CTRL. Solid lines in black, blue, green, and red represent the MSE tendency, OLR, horizontal, and vertical MSE advections, respectively. Dashed lines in light blue, black, and orange indicate latent heat flux, sensible heat flux, and radiative heating, respectively. The MJO convective center is located at 0°.

According to Eq. (1), the moisture tendency is determined by the sum of horizontal moisture advection, vertical moisture advection, and moisture loss (gain) due to condensational heating (evaporation) processes and vertical diffusion.

The diagnosis of vertically integrated (1000–700 hPa) MJO moisture budget indicates that the low-level moistening ahead of the convection arises from anomalous vertical advection (Fig. 4a). Further diagnosis shows that this term is primarily attributed to advection of mean moisture by anomalous ascending motion associated with anomalous low-level convergence. Surface evaporation also shows a positive contribution, while it is about an order of magnitude smaller than the leading term of vertical moisture advection. Both horizontal moisture advection and net condensational heating contribute negatively to the moisture asymmetry. The negative horizontal moisture advection is due to the mean easterly throughout the troposphere in the idealized aquaplanet simulation (Fig. 7d) that advects the perturbation moisture westward. Vertical diffusion produces a negative but negligible effect in the diagnosis (not shown). The net effect of the three budget terms on the right-hand side of Eq. (1) is positive, indicating the dominant role of anomalous vertical moisture advection in causing the moisture zonal asymmetry in the PBL. The result is consistent with the 40-yr European Centre for Medium-Range Weather Forecasts (ECMWF) Re-Analysis (ERA-40) diagnosis by Hsu and Li (2012). The result of column-integrated (1000–100 hPa) moisture budget (Fig. 4b) is in general similar to that of the PBL moisture budget (Fig. 4a). The vertical moisture advection dominates the moistening to the east of the MJO convection center, which is partially offset by the negative horizontal advection and latent heating.

Because the anomalous MSE is primarily regulated by perturbation specific humidity, a maximum MSE anomaly occurs in the middle troposphere. The column-integrated intraseasonal MSE budget analysis shows that radiative heating is approximately in phase with MJO deep convection while vertical advection is nearly out of phase with MJO deep convection (Fig. 5). Previous studies (Maloney 2009; Kiranmayi and Maloney 2011) suggested that horizontal advection dominates the buildup of MSE in advance of MJO convection and, hence, contributes to the eastward propagation of the MJO. However, this effect is not observed in our model because of the strong mean easterly over the tropics produced by the zonally symmetric aquaplanet configuration. The mean easterly advects MSE perturbation westward, inducing a negative horizontal advection of MSE to the east of MJO convection in the model. On the contrary, the perturbation latent heat flux (LHF) contributes to positive MSE tendency ahead of MJO convection as the mean easterly would enhance wind speed to the east of MJO convection. Such contribution is associated with the wind-induced surface heat exchange (WISHE) mechanism (Emanuel 1987; Neelin et al.

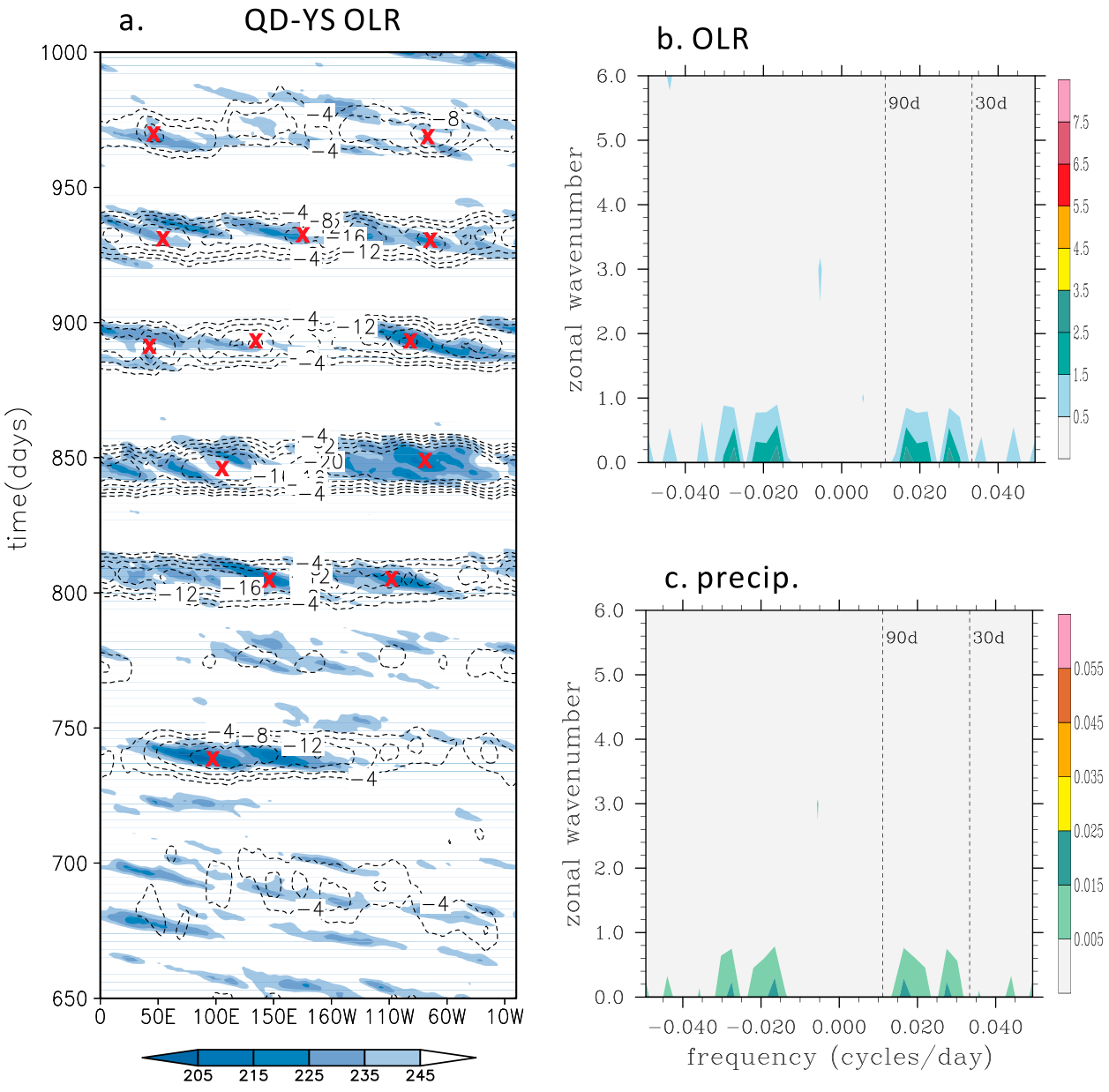

FIG. 6. As in Fig. 1, but for the QD experiment.

1987). Along with the positive LHF anomaly, the column-integrated vertical MSE advection and radiative heating contribute positively to the positive MSE tendency at the transition zone of MJO convection (OLR′ = 0 at around 80°E), favoring the eastward propagation of simulated MJO (Fig. 5).

4. MJO behavior in the *q*-damping experiment

To demonstrate the essential role of the moisture asymmetry in MJO eastward propagation, we conduct a sensitivity experiment (QD experiment) in which we suppress the low-level moisture asymmetry in the aqua-planet AGCM. Figure 6a shows the time–longitude section of OLR at the equator in the QD. The elimination of the lower-tropospheric moisture asymmetry results in a dramatic change in propagation. Both OLR and precipitation appear to be stationary at the equator. The power spectral analysis of equatorial OLR and precipitation fields shows approximately same eastward and westward variances (Figs. 6b and 6c), confirming that the intraseasonal mode is indeed a stationary mode.

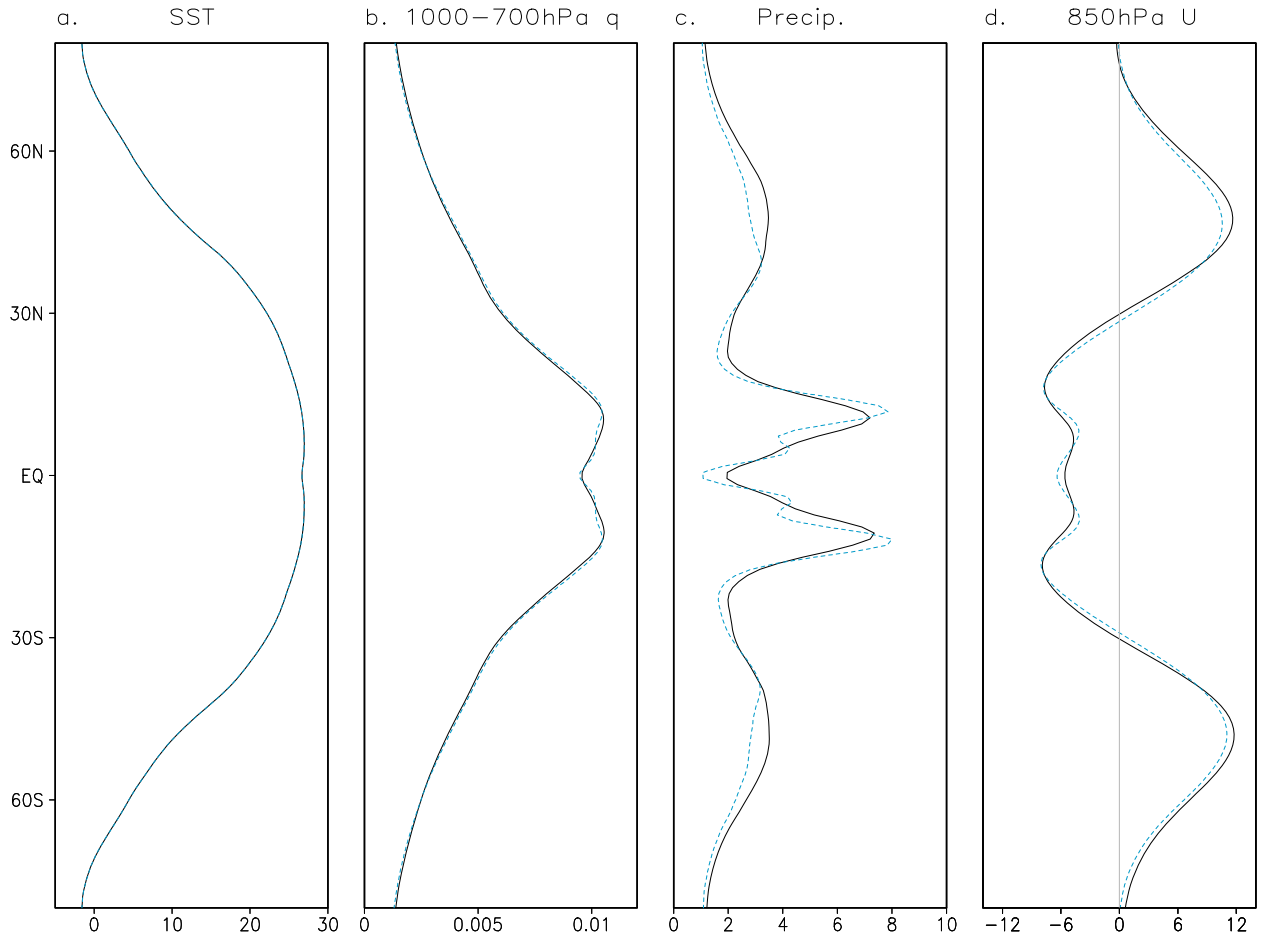

FIG. 7. Latitudinal distributions of zonally averaged (a) SST (°C), (b) 1000–700-hPa mean specific humidity (kg kg^{-1}), (c) precipitation (mm day^{-1}), and (d) 850-hPa zonal wind (m s^{-1}). Black and blue lines represent the CTRL and QD outputs, respectively.

To examine whether the low-level moisture damping causes the mean state change, we compare the time-averaged specific humidity, precipitation and 850-hPa zonal wind fields derived from the CTRL and QD (Fig. 7). It turns out that the climatological mean states in the two experiments are generally similar. Both experiments produce the twin peaks of low-level moisture and precipitation at 10°S and 10°N. The easterly flows are pronounced in the tropics throughout the troposphere. The small change in the mean flow implies that different behaviors between CTRL and QD are primarily attributed to the perturbation moisture asymmetry.

Applying the same methodology as for the CTRL, we select 70 strong convection centers to make a composite to illustrate the zonal phase relationship between the 30–90-day filtered OLR and moisture–convergence fields in the QD (Figs. 8c and 8d). As expected, the composited moisture field is approximately of zonal symmetry (Fig. 8c), in contrast to the asymmetric feature in the CTRL (Fig. 2c). However, the low-level convergence remains of zonal asymmetry (Fig. 8d). This implies that PBL divergence asymmetry alone does not induce the eastward propagation of atmospheric heating. The effect of the PBL convergence on MJO propagation is through its impact on low-level moisture and atmospheric convective instability (Hsu and Li 2012).

The composites of horizontal patterns in the lower and upper troposphere illustrate a baroclinic Kelvin–Rossby wave couplet structure in the QD (Figs. 8a and 8b). This implies that the convectively coupled Kelvin–Rossby wave couplet does not prefer eastward or westward propagation. It is the moisture asymmetry that is essential to cause the eastward propagation.

To test the sensitivity of the model result to the moisture damping coefficient, we carry out additional sensitivity experiments in which different Newtonian damping time scales are used. When a 1-day damping coefficient is applied, the model moisture field has the same zonally symmetric feature (Fig. 9a), as in Fig. 8c.

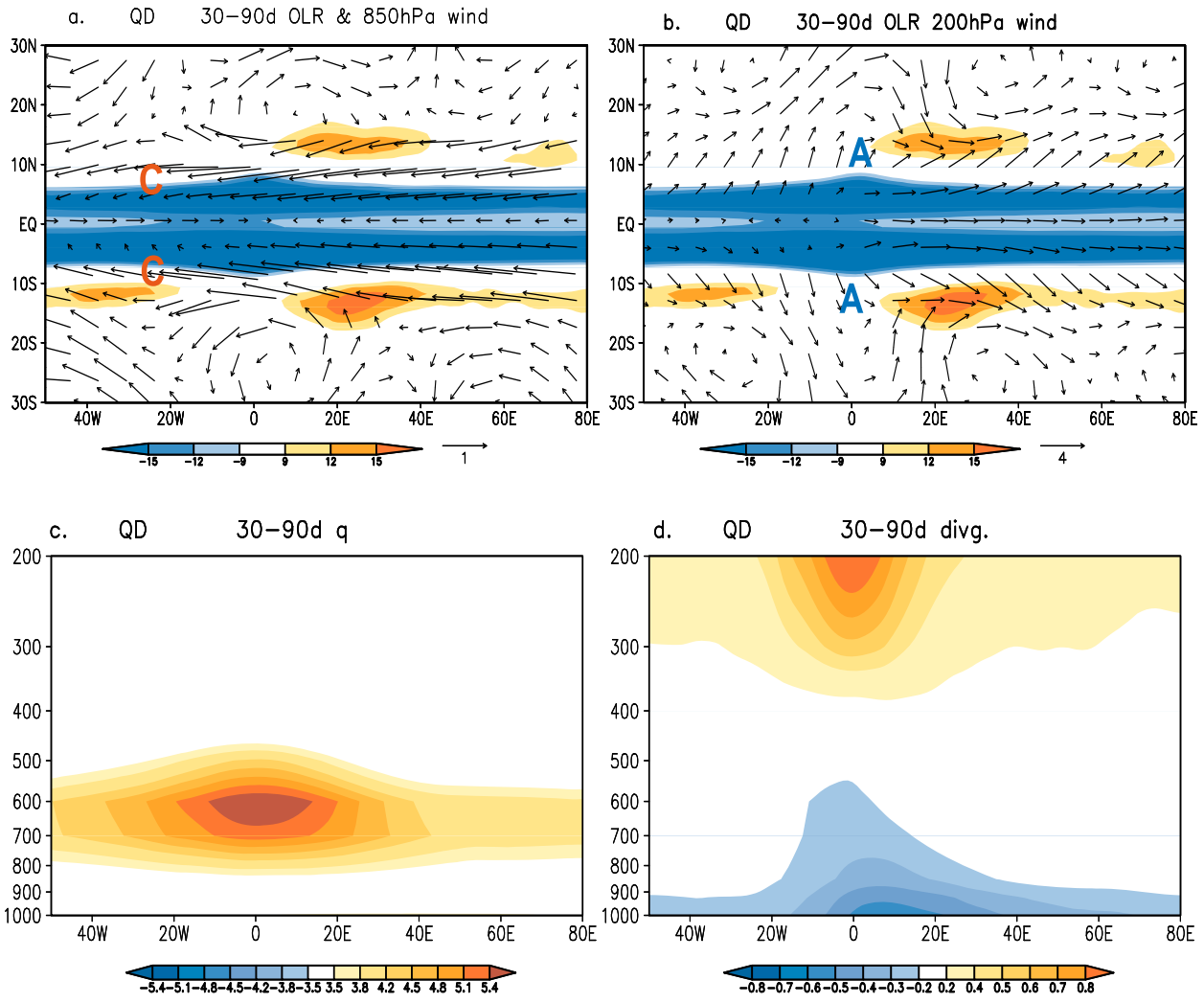

FIG. 8. As in Fig. 2, but for the QD experiment.

As a result, the intraseasonal signals in the model show the same quasi-stationary feature (Fig. 9c), similar to that of the QD with a 0.5-day damping coefficient (Fig. 6a). When a 3-day damping coefficient is applied, the perturbation moisture becomes zonally asymmetric (Fig. 9b). Consequently, the eastward-propagating MJO-like disturbances appear in model (Fig. 9d). The sensitivity experiment supports the conclusion that the moisture zonal asymmetry related to the PBL convergence is essential for generating the eastward propagation of MJO.

5. Sensitivity to convection schemes

Considering that the model MJO may be sensitive to the treatment of convective process in the aquaplanet AGCM, two additional experiments with different cumulus parameterization schemes of the Arakawa–Schubert (AS) scheme and Kain–Fritsch (KF) scheme are conducted. As shown in Fig. 10, the eastward-propagating convection signals were observed in simulations with various convection schemes. Again, the eastward propagation is induced by the leading phase of low-level moistening that causes a relatively unstable stratification to the east of the convection (Fig. 11). The major difference between these experiments lies in their periodicities. The convective perturbations move more slowly (faster) in the model experiments with the AS (KF) scheme as compared to those simulated by the YS scheme (Figs. 1b and 10c,d).

We further conduct QD experiments using the two additional convection schemes. For the QD experiments, regardless of the types of convection scheme, the eastward-propagating convective signals are largely

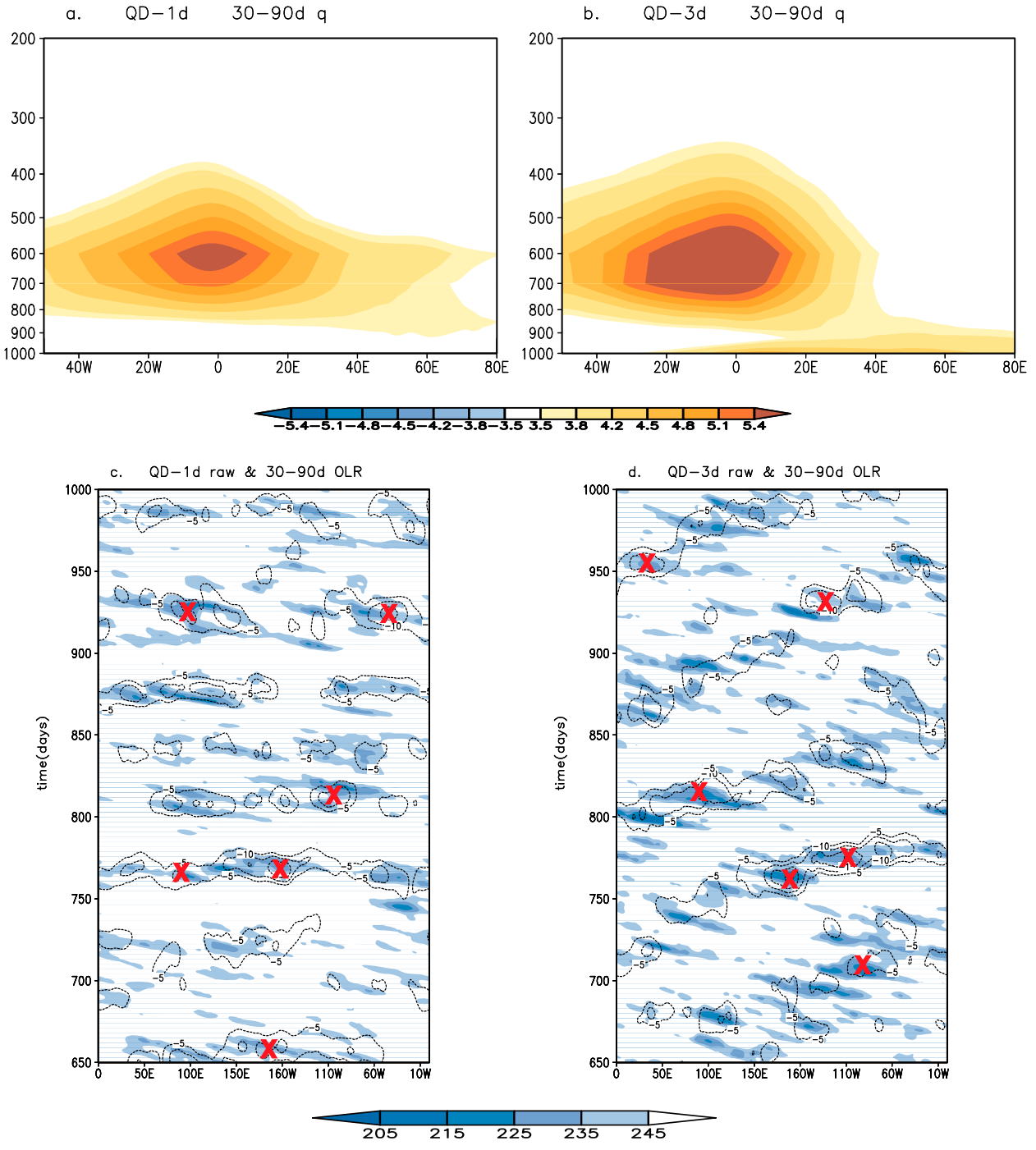

FIG. 9. (top),(bottom) As in Fig. 8c and Fig. 6a, but for the experiments with (a),(c) 1- and (b),(d) 3-day damping coefficients, respectively.

suppressed (Figs. 12a,b). Compared to the spectral analysis results in Figs. 10 and 12, it is found that the large variances in the eastward component shown in the CTRL (Figs. 10c,d) disappear in the QD experiments (Figs. 12c,d). The intraseasonal perturbations become either quasi-stationary (when the KF scheme is used) or westward propagating (when the AS scheme is used). Based on the results of these sensitivity experiments, we conclude that the PBL moisture asymmetry is critical for MJO eastward propagation, and the conclusion is robust and not sensitive to the treatment of convective parameterization.

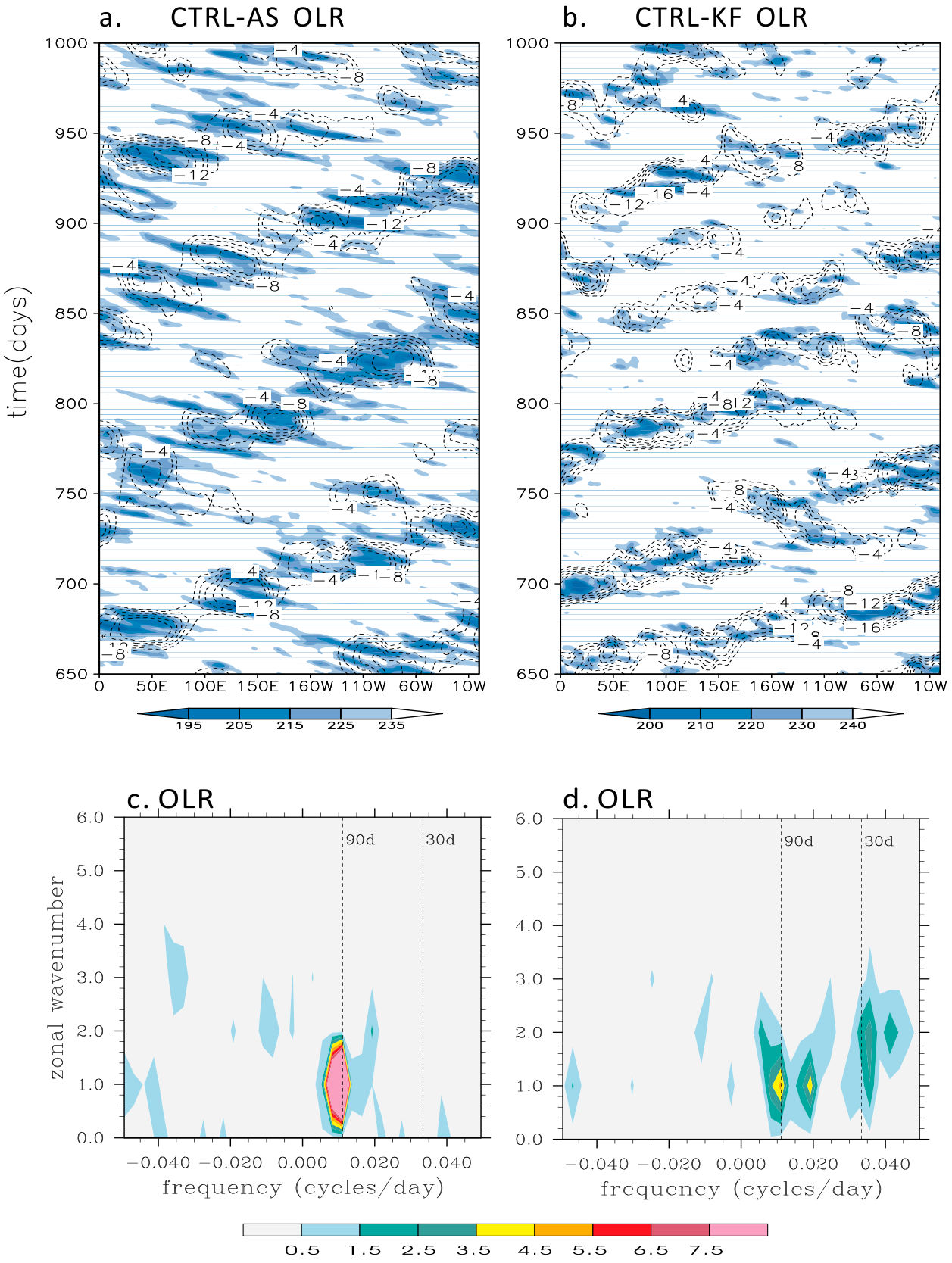

FIG. 10. (top),(bottom) As in Fig. 1a and Fig. 1b, but for the CTRL simulations using (a),(c) the Arakawa–Schubert and (b),(d) the Kain–Fritsch cumulus schemes, respectively.

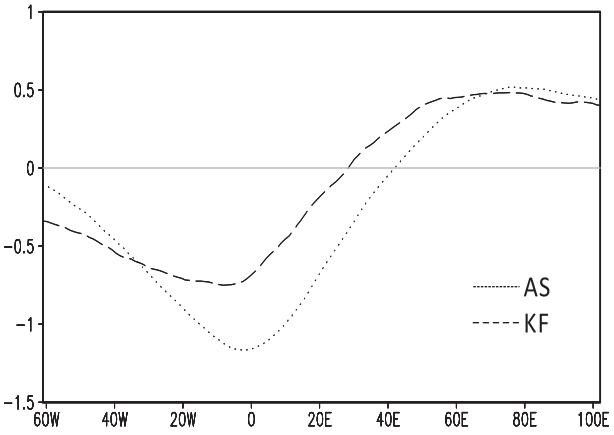

FIG. 11. As in the bottom of Fig. 3, but for the CTRL simulations using the Arakawa–Schubert (dotted) and Kain–Fritsch (dashed) cumulus schemes.

6. Summary and discussion

A slowly eastward-propagating MJO mode with a period of 30–90 days and a zonal wavenumber-1 structure is simulated in an aquaplanet AGCM with a specified zonally and hemispheric symmetric SST distribution. The examination of the model result shows that the simulated 30–90-day perturbations exhibit a Kelvin–Rossby wave couplet structure and vertically tilted moisture and divergence fields, similar to the observed MJO (Salby et al. 1994; Benedict and Randall 2007).

A moisture budget diagnosis indicates that the vertical advection associated with low-level convergence primarily contributes to the PBL moistening ahead of the MJO convection. Although smaller, horizontal advection also contributes positively to the moisture asymmetry in some longitudinal locations in the reanalysis data (Kiranmayi and Maloney 2011; Hsu and Li 2012). However, in the idealized aquaplanet scenario, the horizontal moisture advection plays a negative role in MJO propagation because the mean flows advect the perturbation moisture westward. The negative contribution of horizontal moisture advection in the zonally symmetric aquaplanet simulation is due to 1) pronounced mean easterlies in the tropics that advect anomalous moisture westward and 2) the lacking of mean zonal moisture gradient that can be acted upon by the wind anomalies.

To demonstrate the importance of the moisture asymmetry in the eastward propagation, we conducted a sensitivity experiment in which we forced the lower-tropospheric specific humidity toward a zonal-mean basic state derived from the control simulation. With the zonal moisture asymmetry removed, the low-level convergence asymmetry was still presented. However, the simulated intraseasonal perturbations became quasi-stationary. The idealized numerical experiments demonstrated the important role of the zonal moisture asymmetry in the MJO propagation.

The idealized aquaplanet experiments raise some important theoretical issues related to MJO dynamics. From a wave dynamics point of view, does a convectively coupled Kelvin–Rossby wave couplet move eastward without involving of the moisture zonal asymmetry? So far, there is no theoretical analysis of dispersion relationship for a convectively coupled Kelvin–Rossby wave couplet. From a moisture budget point of view, a key issue is how and to what extent the PBL moisture asymmetry arises from heating-induced free-atmospheric waves. The recent observational analysis of Hsu and Li (2012) pointed out the close connection between the moisture asymmetry and Kelvin wave–induced PBL convergence. Neither the wave dynamics nor the moisture mode alone can cause the MJO propagation. This implies that a ''pure'' moisture mode without coupling with wave dynamics (e.g., Raymond 2001) does not exist.

It is interesting to note that in the 2.5-layer model of Wang and Li (1994) and Li and Wang (1994), eastward-propagating MJO-like signals were simulated, but in their model the perturbation moisture was not considered. We believe that the eastward propagation in the model is attributed to the idealized treatment of convective heating, which is proportional to both lower-tropospheric and PBL convergence. While the lower-tropospheric convergence was in phase with the convective center, the PBL convergence led the convection. As a result, the parameterized heating always appeared to the east of MJO convection in the model, which pulled the system eastward.

It is worth mentioning that the conclusion derived from the current study is based on a single model. It is necessary to conduct similar experiments using different AGCMs to see whether or not the results are sensitive to model physics and configuration. In addition, different SST distributions (with narrower or wider warm pools in the meridional direction, or with maximum SST away from the equator) should be tested to understand the sensitivity of instability and propagation behavior of the convectively coupled Kelvin–Rossby wave couplet to the underlying SST distribution. These experiments will be undertaken in the near future.

Acknowledgments. This work was supported by China National 973 Project 2015CB453200, NSFC Grants 41375100 and 41475084, Natural Science Foundation of Jiangsu Province (BK20140046), Research Project of Chinese Ministry of Education (213014A), NSF Grant

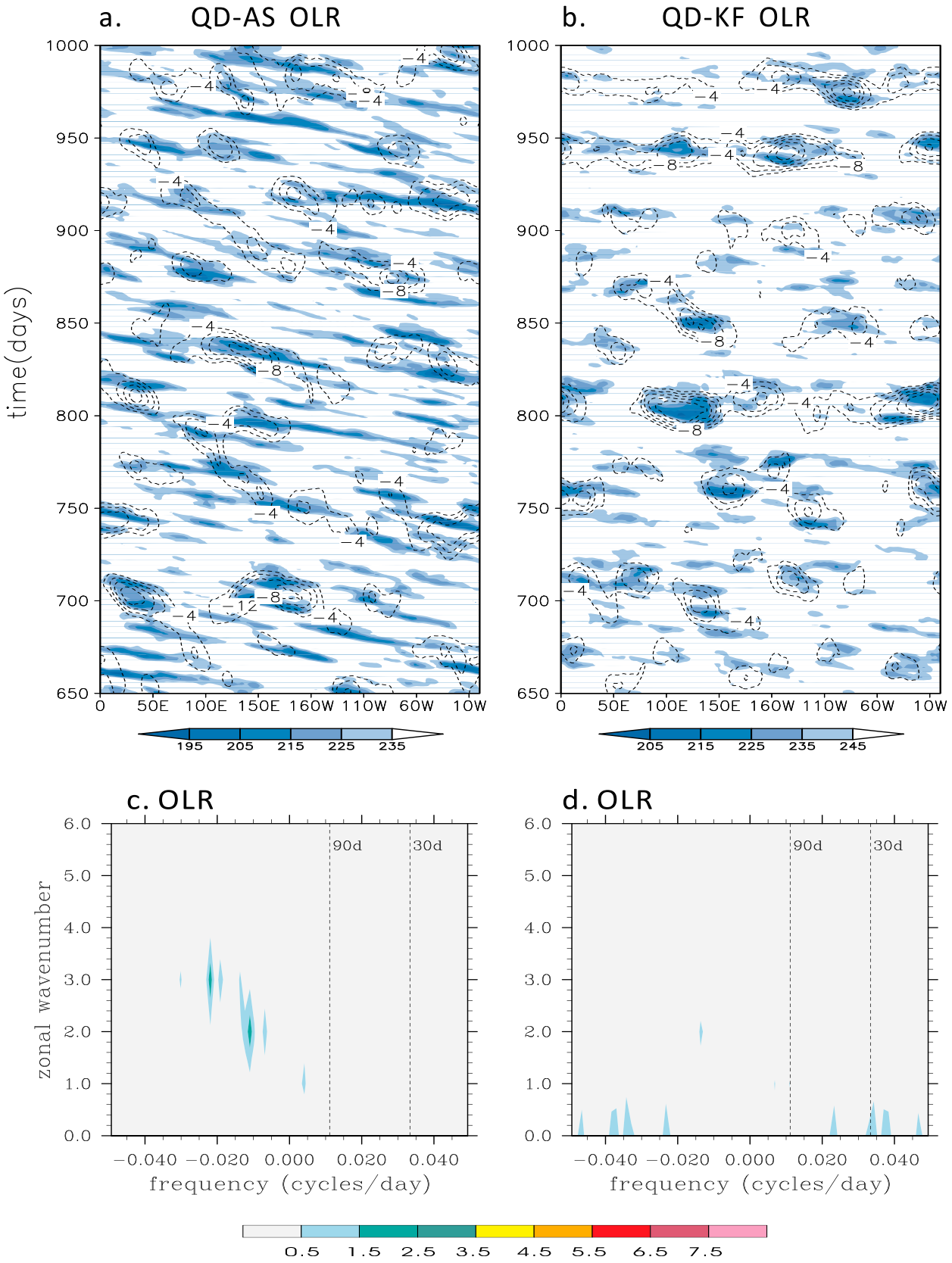

FIG. 12. As in Fig. 10, but for the QD experiments.

AGS-1106536, ONR Grant N00014-1210450, and by the International Pacific Research Center. Comments from three anonymous reviewers are greatly appreciated. The authors thank the modeling groups at the MRI for their help on model experiments. The numerical simulations were performed on the Earth Simulator.

REFERENCES

Andersen, J. A., and Z. Kuang, 2012: Moist static energy budget of MJO-like disturbances in the atmosphere of a zonally symmetric aquaplanet. *J. Climate,* **25,** 2782–2804, doi:10.1175/JCLI-D-11-00168.1.

Arakawa, A., and W. H. Schubert, 1974: Interaction of cumulus cloud ensemble with the large-scale environment, Part I. *J. Atmos. Sci.,* **31,** 674–701, doi:10.1175/1520-0469(1974)031<0674:IOACCE>2.0.CO;2.

Benedict, J., and D. A. Randall, 2007: Observed characteristics of the MJO relative to maximum rainfall. *J. Atmos. Sci.,* **64,** 2332–2354, doi:10.1175/JAS3968.1.

Emanuel, K. A., 1987: An air–sea interaction model of intraseasonal oscillations in the tropics. *J. Atmos. Sci.,* **44,** 2324–2340, doi:10.1175/1520-0469(1987)044<2324:AASIMO>2.0.CO;2.

Hayashi, Y., and A. Sumi, 1986: The 30–40 day oscillations simulated in an ''aqua-planet'' model. *J. Meteor. Soc. Japan,* **64,** 451–466.

Hendon, H. H., and M. L. Salby, 1994: The life cycle of Madden–Julian Oscillation. *J. Atmos. Sci.,* **51,** 2225–2237, doi:10.1175/1520-0469(1994)051<2225:TLCOTM>2.0.CO;2.

Hsu, P.-C., and T. Li, 2012: Role of the boundary layer moisture asymmetry in causing the eastward propagation of the Madden–Julian oscillation. *J. Climate,* **25,** 4914–4931, doi:10.1175/JCLI-D-11-00310.1.

Kemball-Cook, S. R., and B. C. Weare, 2001: The onset of convection in the Madden–Julian oscillation. *J. Climate,* **14,** 780–793, doi:10.1175/1520-0442(2001)014<0780:TOOCIT>2.0.CO;2.

Kiladis, G. N., K. H. Straub, and P. T. Haertel, 2005: Zonal and vertical structure of the Madden–Julian oscillation. *J. Atmos. Sci.,* **62,** 2790–2809, doi:10.1175/JAS3520.1.

Kiranmayi, L., and E. D. Maloney, 2011: Intraseasonal moist static energy budget in reanalysis data. *J. Geophys. Res.,* **116,** D21117, doi:10.1029/2011JD016031.

Lee, M.-I., I.-S. Kang, and B. E. Mapes, 2003: Impacts of cumulus convection parameterization on aqua-planet AGCM simulations of tropical intraseasonal variability. *J. Meteor. Soc. Japan,* **81,** 963–992, doi:10.2151/jmsj.81.963.

Li, T., 2014: Recent advance in understanding the dynamics of the Madden-Julian oscillation. *J. Meteor. Res.,* **28,** 1–33, doi:10.1007/s13351-014-3087-6.

——, and B. Wang, 1994: The influence of sea surface temperature on the tropical intraseasonal oscillation: A numerical study. *Mon. Wea. Rev.,* **122,** 2349–2362, doi:10.1175/1520-0493(1994)122<2349:TIOSST>2.0.CO;2.

——, and C. Zhou, 2009: Planetary scale selection of the Madden–Julian oscillation. *J. Atmos. Sci.,* **66,** 2429–2443, doi:10.1175/2009JAS2968.1.

Madden, R. A., and P. R. Julian, 1971: Detection of a 40–50 day oscillation in the zonal wind in the tropical Pacific. *J. Atmos. Sci.,* **28,** 702–708, doi:10.1175/1520-0469(1971)028<0702:DOADOI>2.0.CO;2.

——, and ——, 1972: Description of global scale circulation cells in the Tropics with a 40–50 day period. *J. Atmos. Sci.,* **29,** 1109–1123, doi:10.1175/1520-0469(1972)029<1109:DOGSCC>2.0.CO;2.

Maloney, E. D., 2009: The moist static energy budget of a composite tropical intraseasonal oscillation in a climate model. *J. Climate,* **22,** 711–729, doi:10.1175/2008JCLI2542.1.

——, and D. L. Hartmann, 1998: Frictional moisture convergence in a composite life cycle of the Madden–Julian oscillation. *J. Climate,* **11,** 2387–2403, doi:10.1175/1520-0442(1998)011<2387:FMCIAC>2.0.CO;2.

——, A. H. Sobel, and W. M. Hannah, 2010: Intraseasonal variability in an aquaplanet general circulation model. *J. Adv. Model. Earth Syst.,* **2** (5), doi:10.3894/JAMES.2010.2.5.

Mizuta, R., and Coauthors, 2012: Climate simulations using MRI-AGCM3.2 with 20-km grid. *J. Meteor. Soc. Japan,* **90A,** 233–258, doi:10.2151/jmsj.2012-A12.

Nakazawa, T., 1988: Tropical super clusters within intraseasonal variations over the western Pacific. *J. Meteor. Soc. Japan,* **66,** 823–839.

Neelin, J. D., I. M. Held, and K. H. Cook, 1987: Evaporation–wind feedback and low-frequency variability in the tropical atmosphere. *J. Atmos. Sci.,* **44,** 2341–2348, doi:10.1175/1520-0469(1987)044<2341:EWFALF>2.0.CO;2.

Raymond, D. J., 2001: A new model of the Madden–Julian oscillation. *J. Atmos. Sci.,* **58,** 2807–2819, doi:10.1175/1520-0469(2001)058<2807:ANMOTM>2.0.CO;2.

Rayner, N. A., D. E. Parker, E. B. Horton, C. K. Folland, L. V. Alexander, D. P. Rowell, E. C. Kent, and A. Kaplan, 2003: Global analyses of sea surface temperature, sea ice, and night marine air temperature since the late nineteenth century. *J. Geophys. Res.,* **108,** 4407, doi:10.1029/2002JD002670.

Salby, M. L., R. Garcia, and H. H. Hendon, 1994: Planetary-scale circulations in the presence of climatological and wave-induced heating. *J. Atmos. Sci.,* **51,** 2344–2367, doi:10.1175/1520-0469(1994)051<2344:PSCITP>2.0.CO;2.

Sobel, A. H., and E. D. Maloney, 2013: Moisture modes and the eastward propagation of the MJO. *J. Atmos. Sci.,* **70,** 187–192, doi:10.1175/JAS-D-12-0189.1.

Sperber, K. R., 2003: Propagation and the vertical structure of the Madden–Julian oscillation. *Mon. Wea. Rev.,* **131,** 3018–3037, doi:10.1175/1520-0493(2003)131<3018:PATVSO>2.0.CO;2.

Tiedtke, M., 1989: A comprehensive mass flux scheme for cumulus parameterization in large-scale models. *Mon. Wea. Rev.,* **117,** 1779–1800, doi:10.1175/1520-0493(1989)117<1779:ACMFSF>2.0.CO;2.

Wang, B., and H. Rui, 1990: Dynamics of the coupled moist Kelvin–Rossby wave on an equatorial β-plane. *J. Atmos. Sci.,* **47,** 397–413, doi:10.1175/1520-0469(1990)047<0397:DOTCMK>2.0.CO;2.

——, and T. Li, 1994: Convective interaction with boundary-layer dynamics in the development of a tropical intraseasonal system. *J. Atmos. Sci.,* **51,** 1386–1400, doi:10.1175/1520-0469(1994)051<1386:CIWBLD>2.0.CO;2.

Yanai, M., S. Esbensen, and J.-H. Chu, 1973: Determination of bulk properties of tropical cloud clusters from large-scale heat and moisture budgets. *J. Atmos. Sci.,* **30,** 611–627, doi:10.1175/1520-0469(1973)030<0611:DOBPOT>2.0.CO;2.

Yoshimura, H., R. Mizuta, and H. Murakami, 2014: A spectral cumulus parameterization scheme interpolating between two convective updrafts with semi-Lagrangian calculation of transport by compensatory subsidence. *Mon. Wea. Rev.,* doi:10.1175/MWR-D-14-00068.1, in press.